

Accepted Manuscript

Color tuning of cyclometalated 2-phenylbenzo[d]oxazole-based iridium(III) complexes through modification of different N[^]O ancillary ligands

Gao-Nan Li, Cheng-Wei Gao, Hao-Hua Chen, Ting-Ting Chen, Hui Xie, Shuai Lin, Wei Sun, Guang-Ying Chen, Zhi-Gang Niu

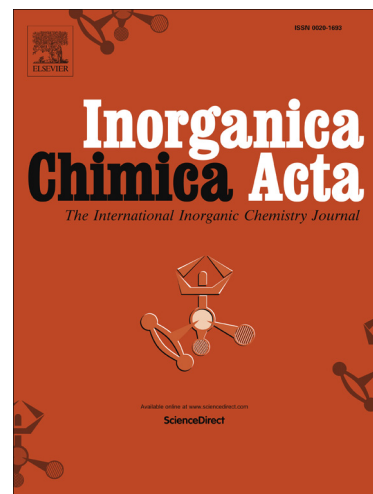
PII: S0020-1693(16)30025-1
DOI: <http://dx.doi.org/10.1016/j.ica.2016.02.009>
Reference: ICA 16879

To appear in: *Inorganica Chimica Acta*

Received Date: 13 November 2015
Revised Date: 31 January 2016
Accepted Date: 2 February 2016

Please cite this article as: G-N. Li, C-W. Gao, H-H. Chen, T-T. Chen, H. Xie, S. Lin, W. Sun, G-Y. Chen, Z-G. Niu, Color tuning of cyclometalated 2-phenylbenzo[d]oxazole-based iridium(III) complexes through modification of different N[^]O ancillary ligands, *Inorganica Chimica Acta* (2016), doi: <http://dx.doi.org/10.1016/j.ica.2016.02.009>

This is a PDF file of an unedited manuscript that has been accepted for publication. As a service to our customers we are providing this early version of the manuscript. The manuscript will undergo copyediting, typesetting, and review of the resulting proof before it is published in its final form. Please note that during the production process errors may be discovered which could affect the content, and all legal disclaimers that apply to the journal pertain.



Color tuning of cyclometalated 2-phenylbenzo[d]oxazole-based iridium(III) complexes through modification of different N^O ancillary ligands

Gao-Nan Li ^{a,1}, Cheng-Wei Gao ^{a,1}, Hao-Hua Chen ^a, Ting-Ting Chen ^a, Hui Xie ^a, Shuai Lin ^a, Wei-Sun ^a, Guang-Ying Chen ^b, Zhi-Gang Niu ^{a,b,*}

^a College of Chemistry and Chemical Engineering, Hainan Normal University, Haikou 571158, China

^b Key Laboratory of Tropical Medicinal Plant Chemistry of Ministry of Education, Hainan Normal University, Haikou 571158, China

Abstract: Four new cyclometalated bo-based iridium(III) complexes with different N^O ancillary ligands, [Ir(bo)₂pic] (**1**), [Ir(bo)₂prz] (**2**), [Ir(bo)₂bop] (**3**) and [Ir(bo)₂btp] (**4**) (bo = 2-phenylbenzo[d]oxazole, pic = picolinate, prz = pyrazinate, bop = 2-benzoxazol-2-yl phenol, btp = 2-benzothiazol-2-yl phenol), have been synthesized and investigated by optical spectroscopy, electrochemistry as well as density functional theory (DFT). The crystal structures of **1**, **2** and **4** have been determined, which show that each adopts the distorted octahedral coordination geometry. They exhibit intense green to orange phosphorescence (λ_{\max} = 531–598 nm) with quantum yields of 0.19–0.94 and lifetimes of 0.078–0.468 μ s in solution at 298 K. The broad range color tuning of complexes **1–4** is dependent on the ancillary ligand structure. The cyclic voltammetry was measured, showing a quasireversible, metal-centered oxidation with potentials at 1.00–1.49 V. The frontier molecular orbital diagrams and the lowest-energy electronic transitions of **1–4** have been calculated with density functional theory (DFT) and time-dependent DFT (TD-DFT).

Keywords: Iridium(III) complex; 2-phenylbenzo[d]oxazole; Ancillary ligand;

* Corresponding author. Tel.: +86 898 31381637; fax: +86 898 65889422.

E-mail address: niuzhigang1982@126.com (Z.-G. Niu).

¹These authors contributed equally to this work.

Photoluminescence; DFT calculation

1. Introduction

In recent years, a considerable amount of interests have been drawn to the application of iridium(III) complexes in organic light-emitting devices (OLEDs), because of their saturated phosphorescence color, high phosphorescence efficiency, and physical compatibility [1-4]. Particularly, well-defined molecular design methods for efficient phosphorescence color tuning are currently under active investigation with the aim of achieving full-color displays [5]. Previous researches found that the emission color of the heteroleptic iridium complexes $[\text{Ir}(\text{C}^{\wedge}\text{N})_2(\text{LX})]$ are largely governed by the nature of the cyclometalated ligands ($\text{C}^{\wedge}\text{N}$), while the ancillary ligand (LX) operated insignificant control [6-8]. But such a standpoint has been changed. Using appropriate ancillary ligands can also achieve the tuning of emission colors for Ir(III) based complexes [9]. For example, the emissions of $\text{Ir}(\text{dfppy})_2(\text{LX})$ [10] can be tuned from blue to red by changing ancillary ligands. Afterward, a series of $\text{Ir}(\text{dfppy})_2(\text{N}^{\wedge}\text{O})$ and $\text{Ir}[(\text{RO})_2\text{pypy}]_2(\text{N}^{\wedge}\text{O})$ heteroleptic iridium(III) complexes were reported, exhibiting intense blue to yellow phosphorescence by changing $\text{N}^{\wedge}\text{O}$ ligands [11]. More recently, we explored the influence of three different hetero-atom (S, O and N) ancillary ligands on the photophysical and electrochemical properties of $[\text{Ir}(\text{btp})_2(\text{LX})]$ iridium(III) complexes [12]. These research support that the ability to tune the emission color by varying the structure of ancillary ligands.

Iridium(III) complex with bis(2-phenylbenzo[d]oxazole) as the ligand, $\text{Ir}(\text{bo})_2(\text{acac})$, was first reported by Thompson et al. [13]. Subsequently, Chen et al. [14] studied $\text{Ir}(\text{bo})_2(\text{acac})$ derivatives with substituents in phenyl ring and showed that the emissive colors of the materials can be finely tuned by systematic control of the nature and position of the substituents on the ligands. Very recently, we also reported $\text{Ir}(\text{bo})_2(\text{acac})$ derivatives with substituents on the benzoxazole ring and obtained a high phosphorescent iridium(III) complex with quantum yields of 53.5% [15].

The above results hence inspired us to further investigate the color tuning of bo-based iridium(III) complexes by choosing different ancillary ligands. Here, we

design four heteroleptic iridium(III) complexes (**1–4**) with bo ligand as the parent compound and pic/prz/bop/btp ancillary ligands as tunable phosphors (Scheme 1). And, their photophysical and electrochemical properties are discussed in detail. The absorption spectra are rationalized on the basis of density functional theory (DFT) and time-dependent DFT (TDDFT).

2. Experimental

2.1. Physical measurements

¹H NMR spectra were recorded on a Bruker AM 400 MHz instrument. Chemical shifts were reported in ppm relative to Me₄Si as internal standard. MALDI-TOF-MS spectra were recorded on a Bruker Autoflex ^{II}TM TOF/TOF instrument. The elemental analyses were performed on a Vario EL Cube Analyzer system. UV-vis spectra were recorded on a Hitachi U3900/3900H spectrophotometer. Fluorescence spectra were carried out on a Hitachi F-7000 spectrophotometer. Luminescence lifetime curves were measured on an Edinburgh Instruments FLS920P fluorescence spectrometer and the data were treated as one-order exponential fitting using OriginPro 8 software.

The luminescence quantum efficiencies were calculated by comparison of the fluorescence intensities (integrated areas) of a standard sample Ir(ppy)₃ and the unknown sample according to the equation [16-17].

$$\Phi_{unk} = \Phi_{std} \left(\frac{I_{unk}}{I_{std}} \right) \left(\frac{A_{std}}{A_{unk}} \right) \left(\frac{\eta_{unk}}{\eta_{std}} \right)^2$$

Where Φ_{unk} and Φ_{std} are the luminescence quantum yield values of the unknown sample and Ir(ppy)₃ solutions ($\Phi_{std} = 1.0$) [11], respectively. I_{unk} and I_{std} are the integrated fluorescence intensities of the unknown sample and Ir(ppy)₃ solutions, respectively. A_{unk} and A_{std} are the absorbance values of the unknown sample and Ir(ppy)₃ solutions at their excitation wavelengths, respectively. The η_{unk} and η_{std} terms represent the refractive indices of the corresponding solvents (pure solvents were assumed).

2.2. Synthesis of ligand

Picolinate (pic) and pyrazinate (prz) were purchased from Energy Chemical.

2-phenylbenzo[d]oxazole (bo) [18], 2-benzoxazol-2-yl phenol (bop) [19], 2-benzothiazol-2-yl phenol (btp) [20] were synthesized according to modification of literature procedures.

2.3. Synthesis of iridium complexes

The dichlorobridged iridium dimer $(bo)_2Ir(\mu-Cl)_2Ir(bo)_2$ was the critical precursor to synthesize complexes **1–4** and prepared according to the literature method [21]. A mixture of $IrCl_3 \cdot 3H_2O$ (1.0 equiv) and bo (2.2 equiv) in a mixture of 2-ethoxyethanol/ H_2O (2:1, v/v) was refluxed for 12 h under nitrogen atmosphere. After cooling, the yellow solid precipitate was collected, washed with H_2O , EtOH and *n*-hexane. The cyclometalated Ir(III) chloro-bridged dimer was used directly in next step without further purification.

2.3.1. Synthesis of $[Ir(bo)_2pic]$ (**1**)

A solution of ancillary ligand pic (0.5 mmol) and dichlorobridged iridium dimer $(bo)_2IrCl_2Ir(bo)_2$ (0.2 mmol), and Na_2CO_3 (1.0 mmol) in 2-ethoxyethanol was refluxed for 24 h. After the mixture was cooled to room temperature, the solvent was evaporated. The residue was purified by column chromatography to give the pure product **1**. Yield: 52%. 1H NMR (400 MHz, $CDCl_3$): δ 8.22 (d, $J = 8.0$ Hz, 1H), 7.95~7.99 (m, 2H), 7.82 (d, $J = 7.6$ Hz, 1H), 7.79 (d, $J = 7.6$ Hz, 1H), 7.72 (d, $J = 7.6$ Hz, 2H), 7.54 (d, $J = 7.6$ Hz, 1H), 7.35~7.41 (m, 2H), 7.27~7.29 (m, 1H), 7.18 (t, $J = 7.6$ Hz, 1H), 7.09 (t, $J = 7.6$ Hz, 1H), 7.00 (t, $J = 7.6$ Hz, 1H), 6.84~6.91 (m, 2H), 6.50~6.52 (m, 1H), 6.43 (d, $J = 7.6$ Hz, 1H). MS (MALDI-TOF) (m/z): 702.935 $[M+H]^+$. Anal. Calcd for $C_{32}H_{20}IrN_3O_4$ (%): C 54.69, H 2.87, N 5.98; Found: C 54.71, H 2.86, N 5.97.

2.3.2. Synthesis of $[Ir(bo)_2prz]$ (**2**)

Complex **2** was obtained by the method similar to the preparation of **1** using prz instead of pic ligand. Yield: 37%. 1H NMR δ 9.43 (s, 1H), 8.73 (d, $J = 2.8$ Hz, 1H), 8.02 (s, 1H), 7.93~7.95 (m, 1H), 7.64~7.70 (m, 4H), 7.35~7.47 (m, 3H), 7.08 (t, $J = 8.0$ Hz, 1H), 7.04 (t, $J = 7.6$ Hz, 1H), 6.97 (t, $J = 7.6$ Hz, 1H), 6.83~6.91 (m, 2H), 6.68 (d, $J = 7.6$ Hz, 1H), 6.44 (d, $J = 7.6$ Hz, 1H), 5.73 (d, $J = 8.0$ Hz, 1H). MS (MALDI-TOF) (m/z): 703.907 $[M+H]^+$. Anal. Calcd for $C_{31}H_{19}IrN_4O_4$ (%): C 52.91,

H 2.72, N 7.96; Found: C 52.91, H 2.70, N 7.97.

2.3.3. Synthesis of $[Ir(bo)_2bop]$ (**3**)

Complex **3** was obtained by the method similar to the preparation of **1** using bop instead of pic ligand. Yield: 49%. 1H NMR δ 7.93 (dd, $J_1 = 2.0$ Hz, $J_2 = 8.0$ Hz, 1H), 7.68~7.75 (m, 3H), 7.60 (d, $J = 8.0$ Hz, 1H), 7.57 (d, $J = 8.0$ Hz, 1H), 7.48 (d, $J = 8.0$ Hz, 1H), 7.28~7.38 (m, 2H), 7.13~7.24 (m, 3H), 6.95~7.03 (m, 3H), 6.79~6.88 (m, 4H), 6.70 (d, $J = 7.6$ Hz, 1H), 6.41~6.51 (m, 2H), 6.36 (d, $J = 8.0$ Hz, 1H), 6.11 (d, $J = 8.4$ Hz, 1H). MS (MALDI-TOF) (m/z): 791.055 $[M+H]^+$. Anal. Calcd for $C_{39}H_{24}IrN_3O_4$ (%): C 59.23, H 3.06, N 5.31; Found: C 59.22, H 3.07, N 5.30.

2.3.4. Synthesis of $[Ir(bo)_2btp]$ (**4**)

Complex **4** was obtained by the method similar to the preparation of **1** using btp instead of pic ligand. Yield: 51%. 1H NMR δ 7.78~7.81 (m, 2H), 7.71 (d, $J = 7.6$ Hz, 1H), 7.66 (d, $J = 7.2$ Hz, 1H), 7.59 (d, $J = 8.0$ Hz, 1H), 7.55 (d, $J = 8.0$ Hz, 1H), 7.27~7.35 (m, 3H), 7.02~7.23 (m, 5H), 6.81~7.99 (m, 4H), 6.63~6.73 (m, 3H), 6.47 (d, $J = 8.4$ Hz, 1H), 6.35 (d, $J = 7.6$ Hz, 1H), 6.27 (t, $J = 7.6$ Hz, 1H). MS (MALDI-TOF) (m/z): 806.970 $[M+H]^+$. Anal. Calcd for $C_{39}H_{24}IrN_3O_3S$ (%): C 58.05, H 3.00, N 5.21; Found: C 58.06, H 3.02, N 5.19.

2.4. Crystal structure determination

X-ray diffraction data were collected with an Agilent Technologies Gemini A Ultra diffractometer equipped with graphite-monochromated Mo $K\alpha$ radiation ($\lambda = 0.71073$ Å) at room temperature. Data collection and reduction were processed with CrysAlisPro software [22]. The structure was solved and refined using Full-matrix least-squares based on F^2 with program SHELXS-97 and SHELXL-97 [23] within Olex2 [24]. All non-hydrogen atoms were found in alternating difference Fourier syntheses and least-squares refinement cycles and, during the final cycles, refined anisotropically. Hydrogen atoms were placed in calculated positions and refined as riding atoms with a uniform value of U_{iso} .

2.5. Computational details

All calculations were carried out with Gaussian 09 software package [25]. The

density functional theory (DFT) and time-dependent DFT (TD-DFT) were employed with no symmetry constraints to investigate the optimized geometries and electron configurations with the Becke three-parameter Lee-Yang-Parr (B3LYP) hybrid density functional theory [26-28]. The LANL2DZ basis set was used to treat the Ir atom, whereas the 6-31G* basis set was used to treat C, H, N, O and S atoms. Solvent effects were considered within the SCRF (self-consistent reaction field) theory using the polarized continuum model (PCM) approach to model the interaction with the solvent [29-30].

2.6. Cyclic Voltammetry

Cyclic voltammetry (CV) was performed on a CHI 1210B electrochemical workstation, with a glassy carbon electrode as the working electrode, a platinum wire as the counter electrode, an Ag/Ag⁺ electrode as the reference electrode, and 0.1 M *n*-Bu₄NClO₄ as the supporting electrolyte.

3. Results and discussion

3.1. Description of the crystal structure

The structures of complexes **1**, **2** and **4** were determined by X-ray crystallography and the ORTEP diagrams are shown in Fig. 1. The crystallographic data and structure refinement details are listed in Table 1; selected bond lengths and bond angles are collected in Table 2. As shown in Fig.1, the Ir^{III} metal center in each complex adopts the distorted octahedral coordination geometry with the C and N atoms of *bo*-based cyclometalated ligands and the O and N atoms of ancillary ligands. As for **2** and **4**, the *bo* ligands bound the nitrogen atoms are *trans* to one another, while the bound carbon atoms are *cis* with respect to the Ir^{III} center, as previously reported complexes [31-33]. Unusually, in **1** the two cyclometallating nitrogen atoms adopt a *cis* disposition rather than *trans* and hence the apparent effect is the lengthening of the Ir–N bond (Ir1–N2 = 2.167(4) Å). Furthermore, the bond distances coordinated to N[^]O ancillary ligands (Ir–O = 2.051-2.186 Å, Ir–N = 2.117-2.133 Å) are the longest among all the coordination bonds. Besides, the 5-membered N₃–Ir–O₃ chelate angle [78.96(15)° for **1**, 76.49(18)° for **2**] is smaller than 6-membered one [84.6(4)° for **4**]. This may be

related to the rigid effect of the five-membered ring at the metal center [15, 34].

3.2. Electronic absorption spectra

The UV-vis absorption spectra of complexes **1–4** in CH₂Cl₂ solution are depicted in Fig. 2, and the data are provided in Table 3. All Ir(III) complexes yielded similar absorption spectra. Strong absorption bands between 230 and 380 nm are assigned to spin allowed $^1\pi-\pi^*$ ligand-centered (LC) transitions arising from both the cyclometalated and ancillary ligands within each complex. Weaker bands in the range of 380-550 nm are assigned to the mixed spin-allowed $^1\text{MLCT}$ and spin-forbidden $^3\text{MLCT}$ transitions [35-36].

According to the structure of the chromophores, the ancillary ligands can be categorized into two classes, namely **1–2** and **3–4**. In the case of **2**, the introduction of the N substitution at 4-position of the pyridine moiety in ancillary ligand results in a more blue-shifted low-energy band than **1**. While, in comparison with **3**, the lowest lying absorption bands for **4** are red-shifted distinctly. The observed result is dependent on the hetero-atom (O and S) changes of the ancillary ligands.

3.3. Emission properties

Photoluminescence (PL) emission spectra of complexes **1–4** in degassed CH₂Cl₂ solution are displayed in Fig. 3 and the corresponding data are also summarized in Table 3. As shown in Fig. 3, the emission spectra of all complexes exhibit broad emission bands without the vibronic structure, indicating that their emissive excited states have $^3\text{MLCT}$ character rather than ligand-centered (^3LC) character [37-39]. It is clearly noted that the emission color can be tuned from green (531 nm) to orange (598 nm) (Table 3). The above considerable range in emission spectra support that the ancillary ligand has more contributions to the emission maxima [11, 40-41].

Photoluminescent quantum yields (Φ) of **1–4** in dichloromethane solution were measured to be 0.190–0.940 (Table 3) at room temperature by using typical phosphorescent Ir(ppy)₃ as a standard ($\Phi = 1.0$). The quantum efficiency follows the order **1**>**2** and **3**>**4**, respectively, for the two classes of Ir(III) complexes. Remarkably, the emission quantum yield for **1** is 0.940, which makes it distinctive as the most

strongly emissive one in the family of complexes.

Phosphorescence (solution) is observed in all cases with microsecond lifetimes at room temperature, ranging from 0.078 to 0.468 μs (Table 3). These lifetimes are indicative of strong spin-orbit coupling leading to intersystem crossing from the singlet to the triplet state. Hence, we believe that in these complexes the emission originates from the triplet states [42].

3.4. Theoretical calculations

Density functional theory (DFT) and time-dependent DFT (TDDFT) calculations have been performed for complexes **1–4** to gain insights into the lowest-energy electronic transition. For comparison, the most representative molecular frontier orbital distributions and the energy levels of the studied complexes are presented in Fig. 4. The calculated spin-allowed electronic transitions are provided in Table 4, as well as compared with the experimental absorption spectra data. The electron density distributions are summarized in Table 5. In detail, for **1** and **2**, the electron density in HOMO is mainly dominated by iridium atom and cyclometalated ligands, whereas the LUMO/LUMO+1 is mainly located on the cyclometalated and ancillary ligands (Table 5). For complexes **3–4**, the HOMO/HOMO-1 is delocalized over the metal, cyclometalated and ancillary ligand, while the LUMO/LUMO+2 is centered on the cyclometalated and ancillary ligand (Table 5). Compared to complex **1**, the N substitution in **2** stabilizes the HOMO and LUMO energy levels, and the decreasing tendency of the LUMO energy level is more significant than that of HOMO (Fig. 4). In contrast, for other complexes **3–4**, the replacement of O by S atom slightly improves the HOMO and LUMO energy levels (Fig. 4). This phenomena may be rationalized by the fact that the sulfur atom in **4** is more polarizable than the oxygen atom in **3**, consequently leading to an increase of the conjugative effect and hence a smaller π - π^* energy gap [43].

The theory calculations of DFT reveal that the lowest-energy electronic transitions (440 nm for **1**, 410 nm for **2**, 408 nm for **3**, 460 nm for **4**) are arised from HOMO \rightarrow LUMO (**1**), HOMO \rightarrow LUMO+1 (**2**), HOMO-1 \rightarrow LUMO (**3**) and

HOMO→LUMO+2 (4) orbital electronic transitions, respectively (Table 4). The corresponding energy gap is 3.783 eV for **1**, 3.877 eV for **2**, 3.750 eV for **3** and 3.460 eV for **4** (Fig. 3). From the results, it can be seen that the energies of the calculated transitions are in good agreement with the experimentally recorded spectra.

3.5. Electrochemical properties

The electrochemical characteristics of iridium complexes **1–4** were investigated by cyclic voltammetry in CH₂Cl₂ solution (Fig.5). The HOMO energy levels are also estimated and summarized in Table 3. All four complexes exhibit a quasireversible one-electron oxidation wave around 1.00-1.49 V, which is generally assigned to the Ir^{IV}/Ir^{III} oxidation [44]. On the basis of the potentials of the oxidation, the E_{HOMO} values are determined using the relevant equations [45] and the resultant values fall in the range -5.80 to -6.29 eV (Table 3). It can be found that the variation tendency of HOMO obtained from experimental characterization is approximately consistent with those obtained from DFT calculations, that is **1**>**2** and **4**>**3**. This again demonstrates that the introduction of the N substitution at 4-position of the pyridine moiety in ancillary ligands has a marked influence on energy levels, as well as the replacement of O by S at para-position of coordinated N atom in ancillary ligands can improve effectively on the HOMO energy levels [12].

4. Conclusion

In summary, using (bo)₂Ir(μ-Cl)₂Ir(bo)₂ as a starting material and N[^]O chelate ligands (N[^]O = pic, prz, bop and btp) as ancillary ligands, a series of cyclometalated [Ir(bo)₂(N[^]O)] iridium(III) complexes **1–4** have been synthesized and characterized. Their photophysical properties, theoretical calculations and electrochemical behaviors have been examined. X-ray diffraction analysis of complexes **1**, **2** and **4** indicate the coordination of the iridium atoms are distorted octahedral geometry. All Ir(III) complexes exhibit moderate to high emission quantum yields and short phosphorescence lifetimes in the range of several microseconds in dichloromethane solution at room temperature. Their phosphorescent colors can be fine-tuned from green to orange by the control of the ancillary ligand. The theoretical calculations

have also been performed to rationalize the photophysical and electrochemical properties. These experimental results enable us to expand our knowledge of fine tuning capabilities of ancillary ligand and establish a guideline for designing novel phosphorescent molecules.

Acknowledgments

This work was supported by the Natural Science Foundation of Hainan Province (No. 20152017), the Natural Science Foundation of Hainan Province (No. 20152017), the Science and Research Project of Education Department of Hainan Province (No. Hnky2015-27) and Hainan Normal University's Innovation Experiment Program for University Students (No. cxcyxj2015005).

Appendix A. Supplementary material

Crystallographic data (excluding structure factors) for the structural analysis have been deposited with the Cambridge Crystallographic Data Center as supplementary publication Nos. CCDC 1434731 (1), 1434733(2) and 1434734 (4). Copies of the data can be obtained free of charge *via* www.ccdc.ac.uk/conts/retrieving.html (or from The Director, CCDC, 12 Union Road, Cambridge CB2 1EZ, UK, Fax: +44-1223-336-033. E-mail: deposit@ccdc.cam.ac.uk).

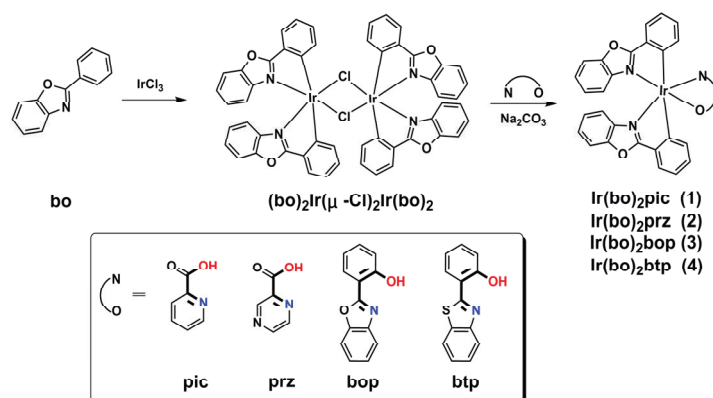
References:

- [1] M.K. Nazeeruddin, R. Humphry-Baker, D. Berner, S. Rivier, L. Zuppiroli, M. Graetzel, *J. Am. Chem. Soc.* 125 (2003) 8790.
- [2] J.M. Lupton, I.D.W. Samuel, M.J. Frampton, R. Beavington, P.L. Burn, *Adv. Funct. Mater.* 11 (2001) 287.
- [3] K.K.M. Lo, C.K. Chung, T.K.M. Lee, L.H. Lui, K.H.K. Tsang, N. Zhu, *Inorg. Chem.* 42 (2003) 6886.
- [4] T. Tsuzuki, N. Shirakawa, T. Suzuki, S. Tokito, *Adv. Mater.* 15 (2003) 1455.
- [5] Y. You, J. Seo, S.H. Kim, K.S. Kim, T.K. Ahn, D. Kim, S.Y. Park, *Inorg. Chem.* 47 (2008) 1476.
- [6] M. Xu, R. Zhou, G. Wang, J. Yu, *Inorg. Chim. Acta* 362 (2009) 2183.
- [7] S.Y. Ahn, H.S. Lee, J. Seo, Y.K. Kim, Y. Ha, *Thin Solid Films* 517 (2009) 4111.
- [8] Y.H. Park, Y.S. kim, *Curr. Appl. Phys.* 7 (2007) 500.

- [9] Y. Hao, X. Guo, L. Lei, J. Yu, H. Xu, B. Xu, *Synth. Met.* 160 (2010) 1210.
- [10] Y. You, S.Y. Park, *J. Am. Chem. Soc.* 127 (2005) 12438.
- [11] H. Oh, K.M. Park, H. Hwang, S. Oh, J.H. Lee, J.S. Lu, S. Wang, Y. Kang, *Organometallics* 32 (2013) 6427.
- [12] G.N. Li, Y.P. Zeng, K.X. Li, H.H. Chen, H. Xie, F.L. Zhang, G.Y. Chen, Z.G. Niu, *J Fluoresc* 26 (2016) 323.
- [13] S. Lamansky, P. Djurovich, D. Murphy, F. Abdel-Razzaq, H.E. Lee, C. Adachi, P.E. Burrows, S.R. Forrest, M.E. Thompson, *J. Am. Chem. Soc.* 123 (2001) 4304.
- [14] H.W. Hong, T.M. Chen, *Mater. Chem. Phys.* 101 (2007) 170.
- [15] Z.G. Niu, T. Zheng, Y.H. Su, P.J. Wang, X.Y. Li, F. Cui, J. Liang, G.N. Li, *New J. Chem.* 39 (2015) 6025.
- [16] A. Juris, V. Balzani, F. Barigelletti, S. Campagna, P. Belser, A. Vonzelewsky, *Coord. Chem. Rev.* 84 (1988) 85.
- [17] M. Frank, M. Nieger, F. Vögtle, P. Belser, A. Vonzelewsky, L.D. Cola, V. Balzani, F. Barigelletti, L. Flamigni, *Inorg. Chim. Acta* 242 (1996) 281.
- [18] Y.T. Leng, F. Yang, W.G. Zhu, Y.J. Wu, X. Li, *Org. Biomol. Chem.* 9 (2011) 5288.
- [19] R.F. Affeldt, A.C.A. Borges, D. Russowsky, F.S. Rodembusch, *New J. Chem.* 38 (2014) 4607.
- [20] K.M. Khan, F. Rahim, S.A. Halim, M. Taha, M. Khan, S. Perveen, Z. Haq, M.A. Mesaik, M.I. Choudhary, *Med. Chem.* 19 (2011) 4286.
- [21] S. Sprouse, K.A. King, P.J. Spellane, R.J. Watts, *J. Am. Chem. Soc.* 106 (1984) 6647.
- [22] CrysAlisPro Version 1.171.36.21. (2012). Agilent Technologies Inc. Santa Clara, CA, USA.
- [23] G.M. Sheldrick, *Acta Cryst.* A64 (2008) 112.
- [24] O.V. Dolomanov, L.J. Bourhis, R.J. Gildea, J.A.K. Howard, H. Puschmann, *J. Appl. Cryst.* 42 (2009) 339.
- [25] M.J. Frisch, G.W. Trucks, H.B. Schlegel, G.E. Scuseria, M.A. Robb, J.R. Cheeseman, J.A. Montgomery, T. Vreven, K.N. Kudin, J.C. Burant, J.M. Millam,

- S.S. Iyengar, J. Tomasi, V. Barone, B. Mennucci, M. Cossi, G. Scalmani, N. Rega, G.A. Petersson, H. Nakatsuji, M. Hada, M. Ehara, K. Toyota, R. Fukuda, J. Hasegawa, M. Ishida, T. Nakajima, Y. Honda, O. Kitao, H. Nakai, M. Klene, X. Li, J.E. Knox, H.P. Hratchian, J.B. Cross, C. Adamo, J. Jaramillo, R. Gomperts, R.E. Stratmann, O. Yazyev, A.J. Austin, R. Cammi, C. Pomelli, J.W. Ochterski, P.Y. Ayala, K. Morokuma, G.A. Voth, P. Salvador, J.J. Dannenberg, V.G. Zakrzewski, S. Dapprich, A.D. Daniels, M.C. Strain, O. Farkas, D.K. Malick, A.D. Rabuck, K. Raghavachari, J.B. Foresman, J.V. Ortiz, Q. Cui, A.G. Baboul, S. Clifford, J. Cioslowski, B.B. Stefanov, G. Liu, A. Liashenko, P. Piskorz, I. Komaromi, R.L. Martin, D.J. Fox, T. Keith, M.A. Al-Laham, C.Y. Peng, A. Nanayakkara, M. Challacombe, P.M.W. Gill, B. Johnson, W. Chen, M.W. Wong, C. Gonzalez, J.A. Pople, Gaussian 09, Revision A.01, Gaussian, Inc. Wallingford, CT, (2009).
- [26] C. Lee, W. Yang, R.G. Parr, *Phys. Rev. B* 37 (1988) 785.
- [27] B. Miehlich, A. Savin, H. Stoll, H. Preuss, *Chem. Phys. Lett.* 157 (1989) 200.
- [28] A.D. Becke, *J. Chem. Phys.* 98 (1993) 5648.
- [29] M. Cossi, N. Rega, G. Scalmani, V. Barone, *J. Comput. Chem.* 24 (2003) 669.
- [30] J. Tomasi, B. Mennucci, R. Cammi, *Chem. Rev.* 105 (2005) 2999.
- [31] Z.G. Niu, D. Liu, J. Zuo, Y. Zou, J.M. Yang, Y.H. Su, Y.D. Yang, G.N. Li, *Inorg. Chem. Commun.* 43 (2014) 146.
- [32] V. Thamilarasan, A. Jayamani, P. Manisankar, Young-Inn Kim, N. Sengottuvelan, *Inorg. Chim. Acta* 408 (2013) 240.
- [33] G.N. Li, Y. Zou, Y.D. Yang, J. Liang, F. Cui, T. Zheng, H. Xie, Z.G. Niu, *J. Fluoresc.* 24 (2014) 1545.
- [34] S. Lamansky, P. Djurovich, D. Murphy, F. Abdel-Razzaq, R. Kwong, I. Tsyba, M. Bortz, B. Mmui, R. Bau, M. E. Thompson, *Inorg. Chem.* 40 (2001) 1704.
- [35] A. Tsuboyama, H. Iwawaki, M. Furugori, T. Mukaide, J. Kamatani, S. Igawa, T. Moriyama, S. Miura, T. Takiguchi, S. Okada, M. Hoshino, K. Ueno, *J. Am. Chem. Soc.* 125 (2003) 12971.
- [36] J.P. Duan, P.P. Sun, C.H. Cheng, *Adv. Mater.* 15 (2003) 224.

- [37] J. Qin, S.Y. Deng, C.X. Qian, T.Y. Li, H.X. Ju, J.L. Zuo, *J. Organomet. Chem.* 750 (2014) 7.
- [38] K.Y. Lu, H.H. Chou, C.H. Hsieh, Y.H. Ou Yang, H.R. Tsai, H.Y. Tsai, L.C. Hsu, C.Y. Chen, I.C. Chen, C.H. Cheng, *Adv. Mater.* 23 (2011) 4933.
- [39] H. Li, Y.M. Yin, H.T. Cao, H.Z. Sun, L. Wang, G.G. Shan, D.X. Zhu, Z.M. Su, W.F. Xie, *J. Organomet. Chem.* 753 (2014) 55.
- [40] H.S. Duan, P.T. Chou, C.C. Hsu, J.Y. Hung, Y. Chi, *Inorg. Chem.* 48 (2009) 6501.
- [41] S.Y. Takizawa, K. Shimada, Y. Sato, S. Murata, *Inorg. Chem.* 53 (2014) 2983.
- [42] M.K. Nazeeruddin, R. Humphry-Baker, D. Berner, S. Rivier, L. Zuppiroli, M. Graetzel, *J. Am. Chem. Soc.* 125 (2003) 8790.
- [43] C.J. Chang, C.H. Yang, K. Chen, Y. Chi, C.F. Shu, M.L. Ho, Y.S. Yeh, P.T. Chou, *Dalton Trans.* (2007) 1881.
- [44] K.R.J. Thomas, M. Velusamy, J.T. Lin, C.H. Chien, Y.T. Tao, Y.S. Wen, Y.H. Hu, P.T. Chou, *Inorg. Chem.* 44 (2005) 5677.
- [45] W. Lee, T. H. Kwon, J. Kwon, J. Y. Kim, C. Lee, J. I. Hong, *New J. Chem.* 35 (2011) 2557.



Scheme 1. Synthetic routes of Ir(III) complexes 1–4.

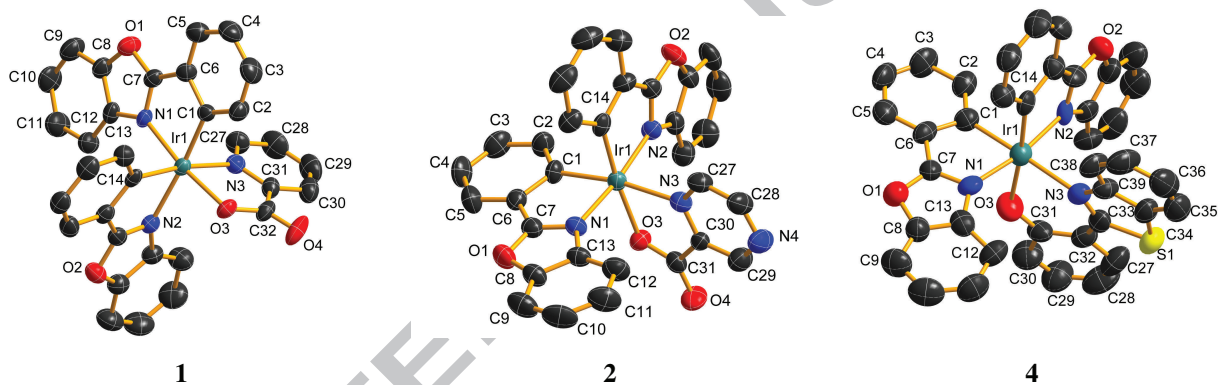
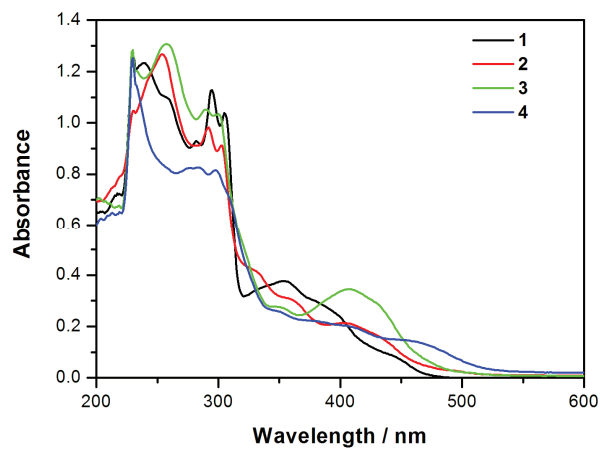


Fig. 1. ORTEP views of 1, 2, 4 with the atom-numbering scheme at the 50% probability level. Hydrogen atoms and solvent molecules are omitted for clarity.

Fig. 2. Electronic absorption spectra of 1–4 in CH_2Cl_2 (2×10^{-5} M) at room temperature.

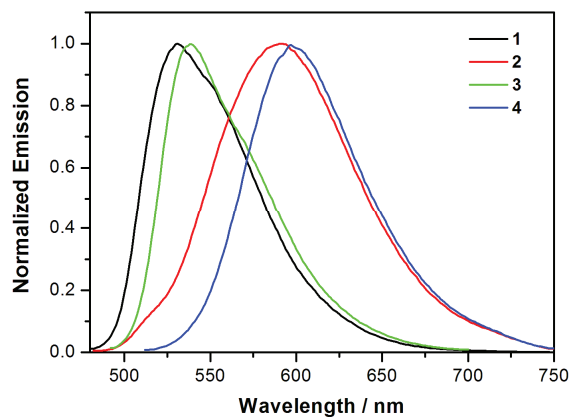


Fig. 3. Normalized emission spectra of 1–4 in CH₂Cl₂ at room temperature.

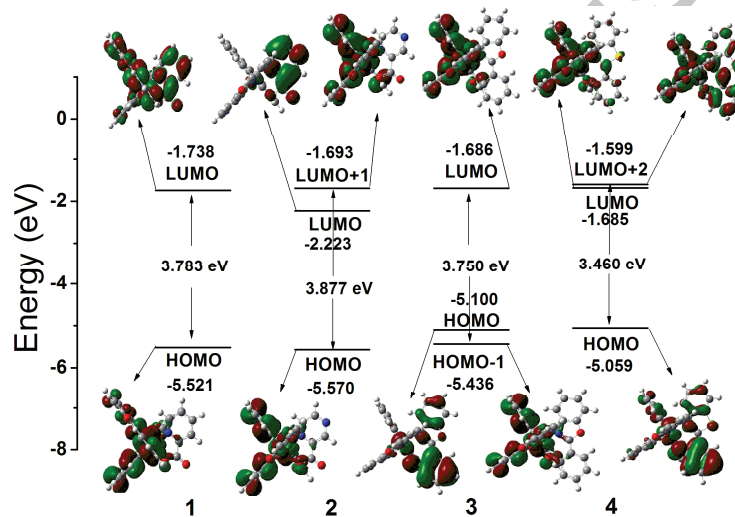


Fig. 4. Molecular orbital energy-level diagrams of complexes 1–4.

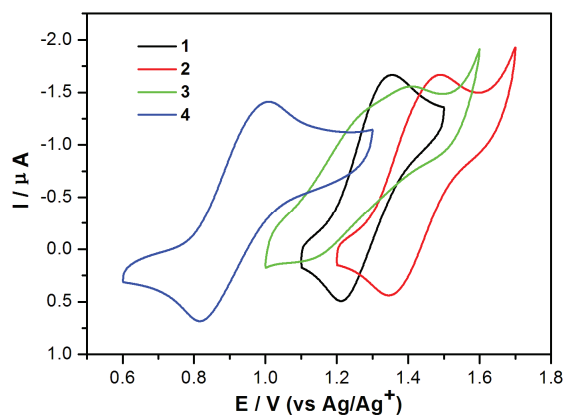


Fig. 5. Cyclic voltammograms for complexes 1–4 in CH₂Cl₂ solution containing *n*-Bu₄NClO₄ (0.1 M) at a sweep rate of 100 mV/s.

Table 1
Crystallographic data for complexes **1**, **2** and **4**.

	1	2·H₂O	4·H₂O
Formula	C ₃₂ H ₂₀ IrN ₃ O ₄	C ₃₁ H ₂₁ IrN ₄ O ₅	C ₃₉ H ₂₆ IrN ₃ O ₄ S
<i>M_r</i>	702.71	721.72	824.89
Crystal system	Monoclinic	Monoclinic	Monoclinic
Space group	<i>P</i> 2 ₁ / <i>c</i>	<i>P</i> 2 ₁ / <i>n</i>	<i>P</i> 2 ₁ / <i>n</i>
Wavelength / Å	0.7107	0.7107	0.7107
X-radiation (graphite monochromator)	Mo-Kα	Mo-Kα	Mo-Kα
<i>T</i> / K	293(2)	293(2)	293(2)
<i>a</i> (Å)	9.9182(4)	10.5183(5)	10.9178(7)
<i>b</i> (Å)	10.5814(4)	17.4162(10)	16.1251(13)
<i>c</i> (Å)	25.3547(11)	14.3974(7)	19.1022(14)
α (°)	90	90	90
β (°)	99.037(4)	93.322(4)	106.168(7)
γ (°)	90	90	90
<i>V</i> (Å ³)	2627.90(18)	2633.0(2)	3230.0(4)
<i>Z</i>	4	4	4
ρ _c (g cm ⁻³)	1.776	1.821	1.696
<i>F</i> (000)	1368	1408	1624
Absorption coefficient / mm ⁻¹	5.125	5.121	4.246
index ranges	-9 ≤ <i>h</i> ≤ 12 -13 ≤ <i>k</i> ≤ 10 -31 ≤ <i>l</i> ≤ 23	-12 ≤ <i>h</i> ≤ 13 -17 ≤ <i>k</i> ≤ 21 -17 ≤ <i>l</i> ≤ 17	-13 ≤ <i>h</i> ≤ 13 -10 ≤ <i>k</i> ≤ 19 -16 ≤ <i>l</i> ≤ 23
GOF (<i>F</i> ²)	1.034	1.039	1.050
<i>R</i> ₁ ^{<i>a</i>} , <i>wR</i> ₂ ^{<i>b</i>} (<i>I</i> > 2σ(<i>I</i>))	0.0338, 0.0675	0.0469, 0.0804	0.0708, 0.1486
<i>R</i> ₁ ^{<i>a</i>} , <i>wR</i> ₂ ^{<i>b</i>} (all data)	0.0452, 0.0724	0.0738, 0.0887	0.1155, 0.1752

^{*a*} *R*₁ = Σ||*F*_o| - |*F*_c||/Σ|*F*_o|. ^{*b*} *wR*₂ = [Σ*w*(*F*_o² - *F*_c²)/Σ*w*(*F*_o²)]^{1/2}

Table 2Selected bond distances (Å) and angles (°) for complexes **1**, **2** and **4**.

1			
Ir(1)-O(3)	2.051(3)	Ir(1)-C(14)	2.044(5)
Ir(1)-N(1)	2.032(4)	N(3)-C(27)	1.334(7)
Ir(1)-N(2)	2.167(4)	N(3)-C(31)	1.346(6)
Ir(1)-N(3)	2.131(4)	O(3)-C(32)	1.292(6)
Ir(1)-C(1)	2.027(5)	O(4)-C(32)	1.220(6)
O(3)-Ir(1)-N(1)	172.18(14)	N(1)-Ir(1)-N(3)	97.77(16)
C(1)-Ir(1)-N(2)	173.40(17)	N(2)-Ir(1)-N(3)	95.71(15)
C(14)-Ir(1)-N(3)	172.08(17)	O(3)-Ir(1)-C(1)	93.56(17)
N(1)-Ir(1)-N(2)	99.47(15)	O(3)-Ir(1)-C(14)	94.61(16)
2			
Ir(1)-O(3)	2.186(4)	Ir(1)-C(14)	2.003(6)
Ir(1)-N(1)	2.043(5)	N(3)-C(27)	1.324(8)
Ir(1)-N(2)	2.030(5)	N(3)-C(30)	1.352(8)
Ir(1)-N(3)	2.117(5)	O(3)-C(31)	1.268(8)
Ir(1)-C(1)	2.022(6)	O(4)-C(31)	1.241(8)
N(2)-Ir(1)-N(1)	173.2(2)	N(3)-Ir(1)-C(14)	99.6(2)
C(14)-Ir(1)-O(3)	174.9(2)	N(1)-Ir(1)-N(3)	94.3(2)
C(1)-Ir(1)-N(3)	170.8(2)	O(3)-Ir(1)-C(1)	95.9(2)
N(1)-Ir(1)-C(14)	95.1(2)	O(3)-Ir(1)-N(2)	97.01(19)
4			
Ir(1)-O(3)	2.129(9)	Ir(1)-C(14)	2.001(12)
Ir(1)-N(1)	2.042(10)	N(3)-C(33)	1.331(15)
Ir(1)-N(2)	2.051(8)	N(3)-C(39)	1.395(14)
Ir(1)-N(3)	2.198(9)	O(3)-C(31)	1.298(15)
Ir(1)-C(1)	2.045(11)	S(1)-C(33)	1.757(13)
N(2)-Ir(1)-N(1)	170.3(4)	C(14)-Ir(1)-N(3)	99.8(4)
C(14)-Ir(1)-O(3)	175.5(4)	N(1)-Ir(1)-N(3)	100.9(4)

C(1)-Ir(1)-N(3)	175.6(4)	O(3)-Ir(1)-C(1)	91.4(4)
C(14)-Ir(1)-N(2)	78.1(4)	O(3)-Ir(1)-N(1)	82.4(4)

Table 3Photophysical and electrochemical data for complexes **1–4**.

Complex	Absorption λ_{abs} (nm) ^a	Emission λ_{em} (nm) ^a	τ / μ s ^a	Φ_{em} ^b	E _{ox} (eV) ^c	HOMO (eV) ^d	HOMO (eV) ^e
1	230, 239, 257, 282, 295, 305, 353, 382, 440	531	0.123	0.940	1.35	-6.15	-5.521
2	230, 254, 291, 302, 333, 361, 410	591	0.078	0.437	1.49	-6.29	-5.570
3	230, 257, 290, 300, 324, 348, 408	539	0.468	0.433	1.40	-6.20	-5.100
4	230, 233, 283, 298, 308, 350, 408, 460	598	0.302	0.190	1.00	-5.80	-5.059

^a Measured in degassed CH₂Cl₂ solution at room temperature. ^b Photoluminescent quantum efficiency measured in CH₂Cl₂, relative to Ir(ppy)₃ ($\Phi = 1.0$).^c Measured in CH₂Cl₂ solution containing 0.1 M *n*-Bu₄NClO₄ and the scan rate was 100 mV/s. ^d HOMO = – (E_{ox} + 4.8 eV). ^e Obtained from theoretical calculations.**Table 4**Main experimental and calculated optical transitions for complexes **1–4**.

Complex	Orbital Excitations	Nature of Transition	Oscillation Strength	Calcd (nm)	Exptl (nm)
1	HOMO → LUMO	Ir(dπ)/L _{bo} (π) → L _{bo/pic} (π [*])	0.0564	414	440
2	HOMO → LUMO+1	Ir(dπ)/L _{bo} (π) → L _{bo} (π [*])	0.1063	409	410
3	HOMO-1 → LUMO	Ir(dπ)/L _{bo} (π) → L _{bo} (π [*])	0.1054	412	408
4	HOMO → LUMO+2	Ir(dπ)/L _{btp} (π) → L _{bo/btp} (π [*])	0.0932	436	460

Table 5Frontier orbital energy and electron density distribution for complexes **1–4**.

Complex	Orbital	Energy (eV)	Composition (%)		
			Ir	cyclometalated ligands	ancillary ligands
1	LUMO	-1.738	1.40	60.08	38.52
	HOMO	-5.521	49.96	45.94	4.10
2	LUMO+1	-1.693	3.61	94.05	2.34
	LUMO	-2.223	3.97	3.54	92.49
3	HOMO	-5.570	48.30	46.55	5.15
	LUMO	-1.686	2.53	94.92	2.54

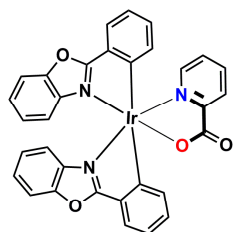
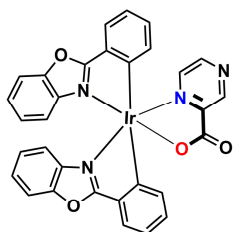
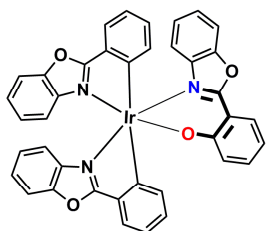
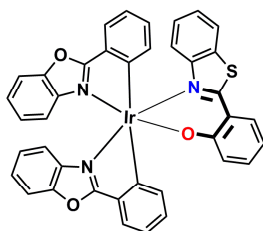
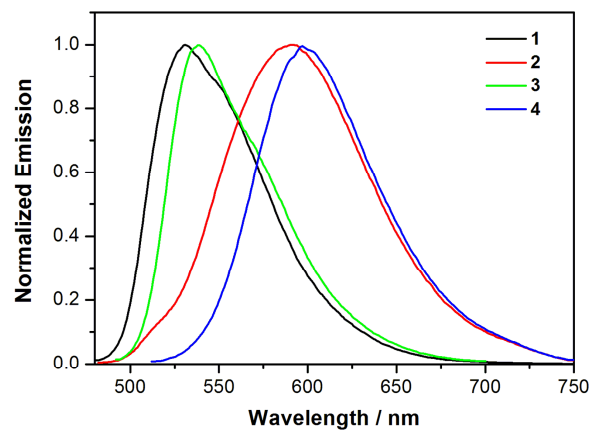
	HOMO	-5.100	19.09	6.93	73.98
	HOMO-1	-5.436	51.46	42.46	6.08
4	LUMO+2	-1.599	3.16	59.86	36.99
	LUMO	-1.685	2.76	87.16	10.07
	HOMO	-5.059	24.15	11.41	64.44

ACCEPTED MANUSCRIPT

GRAPHIC ABSTRACT

Four new cyclometalated iridium(III) complexes $[\text{Ir}(\text{bo})_2(\text{N}^{\wedge}\text{O})]$ (**1-4**) ($\text{N}^{\wedge}\text{O}$ = pic, prz, bop and btp) have been synthesized and fully characterized. The photophysical and electrochemical properties of all complexes have been investigated, and the lowest-energy electronic transitions of absorption spectra have been analyzed by means of time-dependent density functional theory (TD-DFT).

Graphic Abstract-Pictogram

Ir(bo)₂pic (1)Ir(bo)₂prz (2)Ir(bo)₂bop (3)Ir(bo)₂btp (4)

Research Highlights

- Four cyclometalated $[\text{Ir}(\text{bo})_2(\text{N}^{\wedge}\text{O})]$ complexes are synthesized.
- Crystal structures of complexes 1, 2 and 4 are obtained.
- The phosphorescent color tuning is dependent on the ancillary ligand structure.
- The lowest-energy electronic transitions of absorption spectra are analyzed on the basis of DFT and TD-DFT.

ACCEPTED MANUSCRIPT